ChemCatChem

Research Article
doi.org/10.1002/cctc.70141

Chemistry Europe
European Chemical Societies Publishing

www.chemcatchem.org

Glutathione Threshold-Triggered Selective Breakability of Organosilica Nanocapsules

Andrea Mosseri,[a, b, c, d] Ana Rueda-Flores,[a, b] Jose L. Hueso,*[a, b, c, d, e] Esteban Urriolabeitia,[f] Luisa De Cola,[g, h] and Jesus Santamaria*[a, b, c, d]

Biomolecules like proteins and enzymes can target and disrupt cancer cell pathways more specifically and with lower toxicity than traditional treatments. However, their lack of stability and methods for their effective delivery still present unsolved challenges. Silica nanocapsules have been proposed as carriers capable of protecting sensitive loads but their use is limited by their low biodegradability. For this reason, breakable silica structures, able to disassemble when exposed to representative levels of biomolecules readily available in the tumor microenvironment (TME), appear as ideal delivery vectors. In this work, we focus on the optimization of the synthesis parameters governing the breakability of organo-silica nanocapsules containing cleavable disulfide bonds. The objective is to trigger selective release in the presence of glutathione (GSH), a key molecule overexpressed in tumor cells. However, disulfide bonds can also be degraded in the presence of other molecules, which reduces the selectivity of delivery. We have modified the synthesis to obtain a response that leads to silica disassembly only when GSH levels are above a certain threshold, while remaining stable against other reductants, such as those present in standard extracellular culture media. The selection of the proper silica precursor was critical to obtain silica capsules that is able to disassemble and release Cytochrome C (CytC) upon exposure to GSH concentrations typical of those existing in the TME.

1. Introduction

Cancer remains a global health concern, with projections by the World Health Organization (WHO) anticipating a 60% increase in global cancer mortality over the next two decades D. Current therapeutic approaches for cancer include surgery, radiation therapy (RT), chemotherapy (CT), photodynamic therapy (PTT), immunotherapy (IT), and targeted therapy[1] among others. However, despite advancements in these areas, resistance to therapy, recurrence, and adverse effects persist stressing the need for continued research into more effective and personalized therapeutic strategies. Nanomedicine, the health branch of nanotechnology, has spanned a number of different therapeutic strategies against cancer. Among them, the development of smart capsules to achieve efficient and selective delivery of therapeutic cargoes represents one of the major contributions of this interdisciplinary field.[2] In addition, the fabrication and delivery of active catalysts able to disrupt the tumor microenvironment (TME) attracts increasing interest in the field of nanocatalytic medicine as an alternative to the delivery of drugs themselves.[3] A wide plethora of catalysts have been successfully tested to directly disrupt cancer cells by tackling key metabolites,[4] generate reactive oxygen species (ROS),[5] or bioorthogonally activate protected drugs.[4c,6] In a different approach, protein-based drugs are emerging as a powerful alternative in treating cancer, metabolic disorders, and immunological diseases.[7] Protein-based therapy offers distinct advantages over CT and gene therapy (GT). Protein-based drugs exhibit a high specificity

[a] A. Mosseri, A. Rueda-Flores, Dr. J. L. Hueso, Prof. J. Santamaria
Instituto de Nanociencia y Materiales de Aragon (INMA), CSIC-Universidad de Zaragoza, Campus Río Ebro, Edificio I+D, C/ Poeta Mariano Esquillor, s/n, Zaragoza 50018, Spain
E-mail: jlhueso@unizar.es
Jesus.Santamaria@unizar.es

[b] A. Mosseri, A. Rueda-Flores, Dr. J. L. Hueso, Prof. J. Santamaria
Department of Chemical and Environmental Engineering, University of Zaragoza, Campus Río Ebro, C/ María de Luna, 3, Zaragoza 50018, Spain

[c] A. Mosseri, Dr. J. L. Hueso, Prof. J. Santamaria
Networking Research Center in Biomaterials, Bioengineering and Nanomedicine (CIBER-BBN), Instituto de Salud Carlos III, Madrid 28029, Spain

[d] A. Mosseri, Dr. J. L. Hueso, Prof. J. Santamaria
Instituto de Investigación Sanitaria (IIS) de Aragón, Avenida San Juan Bosco, 13, Zaragoza 50009, Spain

[e] Dr. J. L. Hueso
Escuela Politécnica Superior, Universidad de Zaragoza, Crta. de Cuarte s/n, Huesca 22071, Spain

[f] Dr. E. Urriolabeitia
Instituto de Síntesis Química y Catálisis Homogénea (ISQCH), CSIC-Universidad de Zaragoza, Zaragoza 50009, Spain

[g] Prof. L. De Cola
Department of Biochemistry and Molecular Pharmacology, Istituto di Ricerche Farmacologiche Mario Negri IRCCS, Via Mario Negri, 2, Milan, Italy

[h] Prof. L. De Cola
Department of Pharmaceutical Science (DISFARM), Università degli Studi di Milano, Milan, Italy

Supporting information for this article is available on the WWW under https://doi.org/10.1002/cctc.70141

to (i) directly induce cancer cell death; (ii) stimulate immune response; or (iii) indirectly inhibit tumor growth.[7] Furthermore, protein therapy is potentially less cytotoxic than CT drugs and less genotoxic than GT. Shorter amino acid sequences, such as peptides, have been also systematically tested due to the readiness of current sequentiation techniques.[8]

Despite these advantages, current efforts to successfully deliver proteins or peptides to specific tissues or cells are still insufficient.[7c,9] Among the main challenges for their clinical translation are instability during blood circulation, degradation by enzymes, and immunogenicity.[7a,8] To address these issues, several delivery systems have been developed to encapsulate, protect, and control the release of proteins or peptides. The approaches tested include physical entrapment, chemical modification, and the use of nanocarriers with multiple functions, aimed at active tumor targeting, deep tumor penetration, and effective cellular uptake.[7c,9] Smart nanocarriers often based on labile structures have also been developed, able to respond to internal or external stimuli, allowing for on-demand protein release at tumor sites or specific subcellular compartments.[7a]

In this regard, silica nanocapsules have been extensively evaluated as carrier platforms for in vivo applications.[10] Over the years, a vast number of synthetic strategies have been explored to improve the therapeutic and diagnostic efficacy/index, reduce off-target toxicity, and adjust the pharmacokinetic drug release profiles.[10e,11] Because of the difficulties that the nonbiodegradability of silica presents for clinical applications, latest efforts have focused on adding breakability features to silica nanocapsules, triggered by different stimuli (such as pH, redox potential, enzyme, light, thermal, etc.).[10e,11b,12] This has enabled highly appealing *on-demand* release of active cargoes.[10b,10c,11a,13] Beyond increasing the selective disassembly of silica capsules under specific stimuli, current efforts are intended to improve the capability to load different biomolecules as active catalysts or as therapeutic drugs.[8,9c,14] The reverse micelle or water-in-oil (w/o) microemulsion system is a homogeneous mixture of oil, water, and surfactant molecules that is isotropic and thermodynamically stable. Within this system, water nanodroplets are formed in the oil phase and act as confined nanoreactors.[15] This strategy has been used to encapsulate positively charged dye molecules within negatively charged silica capsules.[16] In this work, we have focused on the development of silica nanocapsules specifically responsive to a reducing ambient. Previous research by De Cola´s group[10d] demonstrated the possibility of incorporating a disulfide bond into the silica framework to confer stimuli-responsive breakability in the presence of high concentrations of reducing agents such as glutathione (GSH) and sodium borohydride ($NaBH_4$). Reducing agents can interact with the S—S bond, cleaving it with the generation of two thiols (Figure 1), leaving behind fragments of a size small enough to allow renal clearance. Ideally, a preferential response to GSH is desired since this molecule is overexpressed in the TME, where it is used as an antioxidant to achieve redox homeostasis.[17] In this way, selective activation of capsule breakage could be achieved inside the tumor. However, as described in previous works (see Table S1), disulfide bonds can also be degraded by lower levels of GSH than the ones present in tumors. It should be noted that the range of GSH concentrations reported is wide and strongly depends on the analytical techniques and the cell lines used.[4c,6a,18] Moreover, other reductants, such as those present in common biological media like cell culture media (this work), can easily cleave the S—S bond. This has consequences for potential therapeutic use, as the capsules would be degraded on the way to the target, reducing the selectivity of cargo delivery and release. Herein, we present a double micro-emulsion synthesis approach to generate solid SiO_2 capsules that only break upon exposure to GSH levels above a certain threshold while remaining stable against other reductants, such as those present in culture media. In addition, the nonporous silica nanoparticles used allowed us to encapsulate a small protein, Cytochrome C (CytC). A solid diffusion barrier prevents the early release of the cargo and reduces unwanted toxicity in healthy regions. The synthesis has been tuned to produce effective release at GSH concentrations of 5 mM and above, typical of the TME. The cleavage of the disulfide bonds takes place on an already small silica capsule (25 nm), producing small fragments that facilitate in vivo clearance.[19,20]

2. Results and Discussion

2.1. Synthesis of Breakable Silica Nanoparticles Using Tetraethoxy Orthosilicate (TEOS)

We initially synthesized benchmark breakable silica nanocapsules containing CytC as described by Prasetyanto et al.[10d] (Figure 1) yielding a structure with disulfide bonds successfully integrated in the silica framework. The objective was to maintain the integrity of the nanocapsules prior to cellular uptake and trigger the cleavage of redox group to enable the selective release of the peptide only in the presence of molecules characteristic of the TME. As previously described in the literature, the disulfide bond is a moiety susceptible to rupture in the presence of reducing agents.[10c,10d,20a,21] Notably, chemical species such as GSH can cleave the bond reducing disulfide to two thiols (—SH) groups (Figure 1c). In this work, we have explored the integrity of SiO_2 nanocapsules synthesized under different experimental conditions summarized in Table 1 and in the experimental section (vide infra). We have tested these capsules in the presence of GSH (at concentration levels of 5 mM typically mean concentration found by LC–MS analyses in tumor cells[4c,6a]) and also against Dulbecco's Modified Eagle's Medium (DMEM a commonly used cell culture medium containing molecules that can act as reducing agents such as glucose, high concentration of proteins and vitamins, and sodium pyruvate). The synthesis procedure follows a reverse microemulsion approach[10d] using TEOS as silica precursor and bis[3-(triethoxysilyl)propyl] disulfide (BTSPD) as disulfide source. As shown in Figure 1 (see also experimental section) a first organic in water mixture was generated in an aqueous phase containing TEOS/BTSPD and (for the loaded capsules) CytC. Subsequently, a microemulsion was obtained mixing the aqueous fraction with an organic phase containing cyclohexane, *n*-hexanol and Triton-X under magnetic stirring. The

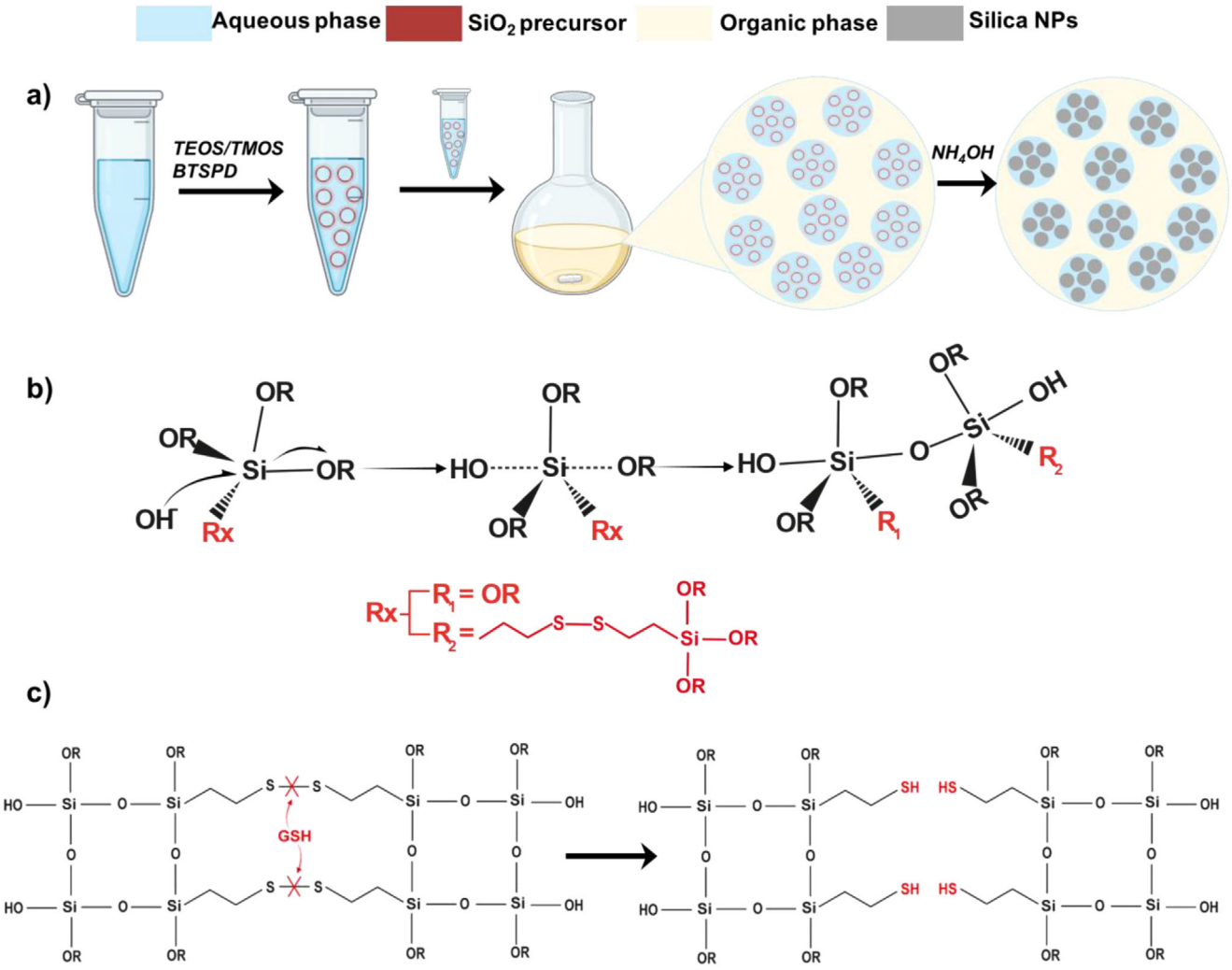

Figure 1. Scheme of the synthesis approach of SiO_2 nanocapsules and GSH cleavage: (a) scheme of synthesis: first step using as aqueous phase double-distilled H_2O (eventually with the CytC dissolved), plus TEOS or TMOS as silica precursor and BTSPD as S—S bond precursor; second step using an organic phase composed by cyclohexane, *n*-hexanol, Triton 100X, and ammonia as catalyst for silica polymerization. (b) Reaction scheme of the polymerization mechanism of silica precursors in basic media. (c) Disulfide bond cleavage induced by GSH to initiate the SiO_2 matrix rupture.

Table 1. Summary of the main precursor concentrations, characterization, and loading tested in this work.

Sample	TEOS or TMOS Volume (μL)	BTSPD[c] Volume (μL)	Ratio[d] SiO_2: S—S	ζ-pot[e] (mV)	Size (nm)	EE[f] (%)	Loading[g] (%)
1-TE[a]	40.0	60.0	1.00: 0.65	−18.3 ± 1.4	23.6 ± 4.7	61.9	6.2
2-TE	40.0	41.5	1.00: 0.45	−10.9 ± 0.4	23.6 ± 4.4	61.3	6.1
3-TE	57.8	60.0	1.00: 0.45	−25.3 ± 2.4	27.1 ± 3.5	60.8	6.1
1-TM[b]	40.0	87.7	1.00: 0.65	−34.8 ± 1.1	18.4 ± 3.0	38.2	3.8
2-TM	40.0	60.0	1.00: 0.45	−37.2 ± 1.4	17.1 ± 2.6	42.1	4.2
3-TM	80.0	120.0	1.00: 0.45	−40.3 ± 2.6	20.2 ± 2.9	58.6	5.9

[a] TE: samples prepared using TEOS.
[b] TM: samples prepared using tetramethoxy orthosilicate (TMOS).
[c] BTSPD: bis[3-(triethoxysilyl)propyl] disulfide.
[d] Molar ratio, expressed as (TEOS or TMOS) moles/BTSPD moles.
[e] Zeta-potential values.
[f] EE: encapsulation efficiency (see experimental section).
[g] CytC loading (wt %/wt.).

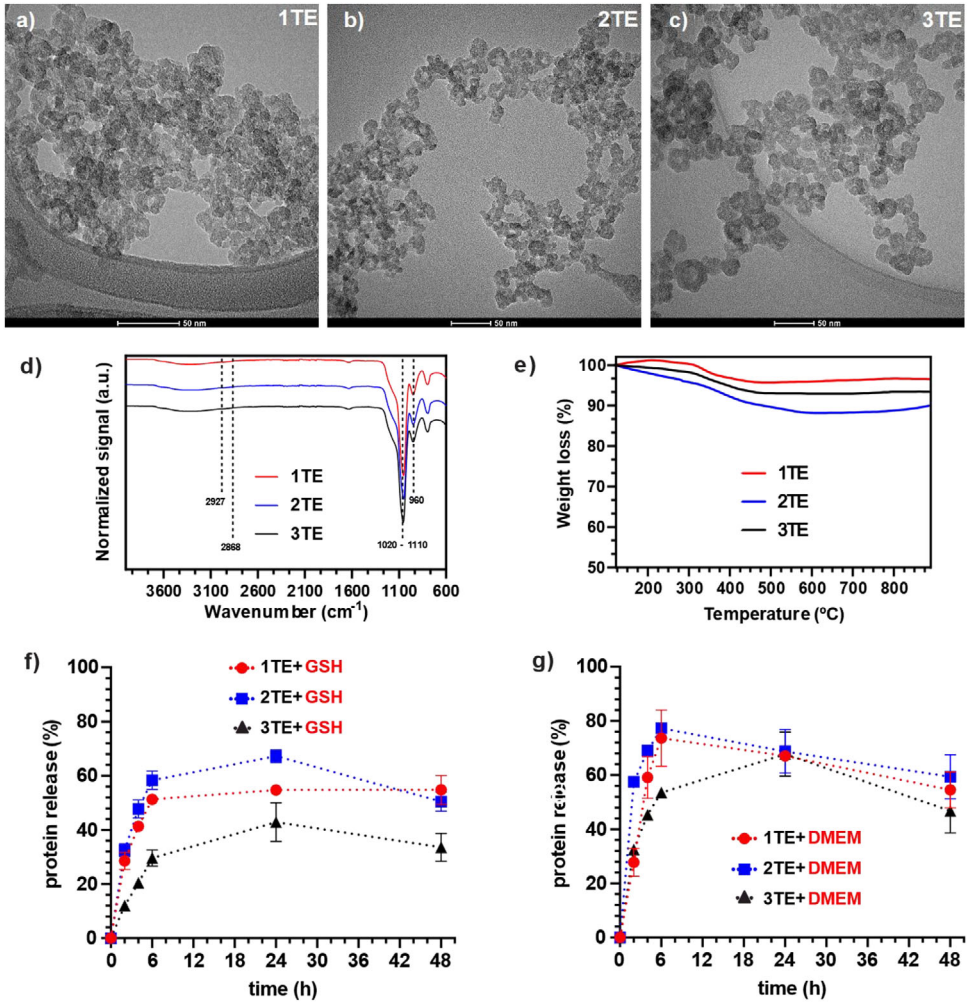

Figure 2. Characterization of TEOS derived silica nanocapsules and release patterns: from (a–c) TEM of organosilica nanoparticles, images at 50 nm scale of syntheses using TEOS as silica precursor (1-TE, 2-TE, 3-TE, respectively). (d) FT-IR analysis of 1-TE, 2-TE, 3-TE. (e) Thermogravimetric analysis of organosilica NPs: syntheses using TEOS as precursor 1-TE (red line), 2-TE (blue line), and 3-TE (black line). (f) Release kinetics of CytC from the different samples 1-TE to 3-TE over 48 h: in the presence of GSH (5 mM in phosphate buffer saline (PBS 0.1 M pH = 7.4). (g) Release kinetics of CytC from the different samples 1-TE to 3-TE over 48 h: in the presence of DMEM (pH = 7.4).

presence of the surfactant (Triton-X) allowed the formation of water-in-oil micelles. The addition of ammonia (NH_4OH), catalyzed silica polymerization, using the micelles as nanoreactors (Figure 1).

All the conditions reported in Table 1 rendered the formation of SiO_2 nanocapsules. Nevertheless, the syntheses using the lower volumes of TEOS and BTSPD (1-TE and 2-TE) led to the generation of nanoparticles, exhibiting some aggregation and defects as revealed by transmission electron microscopy (TEM) analysis (Figure 2a,b). In contrast, an optimal spherical configuration was obtained using higher volumes of both reactants (3-TE, Figure 2c). The particle size distributions derived from TEM and from dynamic light scattering (DLS) measurements were analogous with average sizes around 25 nm (Figure 2a–c, Table 1), zeta potential values became progressively more negative from 1-TE to 3-TE (Table 1). DLS analysis provided hydrodynamic diameters that matched well the TEM measurements, indicating that stable colloidal suspensions were obtained, and the partial aggregation that can be observed under TEM inspection is probably caused by the drying mechanism during grids preparation (Figure S1).

Fourier-transform infrared (FT-IR) analysis (Figure 2e) did not reveal any significant differences. The three TE samples showed analogous spectra (see Figure 2d) with a silica framework characteristic absorption peak at 1020–1110 cm^{-1} assigned to the Si—O—Si asymmetric stretching vibration, and the peaks at 960 cm^{-1} attributed to the asymmetric bending and stretching vibration of Si—OH, respectively. The presence of the S—S bond was accounted by a stretch at 2927–2868 cm^{-1}, slightly visible in the spectra because of the low amount of the chemical bond.[21] Thermogravimetric analyses (TGAs) were useful to elucidate the presence and percentage of disulfide bond. TG curves showed 2.5%–4% weight losses in the range 300–400 °C attributed to the disulfide bond in the structure[10d,20b] (see Figure 2e). The major weight loss was observed in 2-TE. Still, we could estimate that almost 75% BTSPD is not being incorporated in the silica matrix, probably due to its limited miscibility.

2.2. Evaluation of the Breakability and CytC Release in the Silica Nanocapsules Obtained with TEOS

Organosilica nanoparticles containing disulfide bonds in their structure represent a widely studied approach to enhance biodegradation. Several studies employing this strategy improved the biocompatibility and degradation behavior of conventional silica NPs, while also enabling controlled cargo release in redox-rich cancer cell environments.[10d,22] The —S—S— bond is physiologically active and easily degradable, enabling the efficient biodegradation of organosilica frameworks[23] (Figure 1c). In this work, the organosilica nanoparticles synthesis allowed to encapsulate CytC with a loading of 6 wt % and an encapsulation efficiency of 60%, (see Table 1 and experimental section). The breakability of the SiO_2 nanocapsules prepared with TEOS was evaluated after immersing them in a buffered aqueous medium containing GSH (5 mM). Alternatively, the capsules were also evaluated in the presence of DMEM, as a representative culture medium often used in cell studies. All the SiO_2 nanocapsules exhibited similar percentages of protein released and the observed trends were similar both in the presence of GSH and DMEM (Figure 2f,g). Therefore, while the addition of BTSPD was successful in introducing disulfide bonds that led to the degradation of the silica matrix, this rupture was not selective to GSH and took place also in the presence of other reducing molecules. Furthermore, we tried to tune the breakability by changing ratios of the precursor and this had some effect on the total amount of protein released but was not effective in enhancing the role of GSH over DMEM as a disassembly-triggering agent, which was the preferred scenario given its high concentration in the TME.[4c,10d,17a,18a]

2.3. Replacing TEOS by TMOS to Improve the Selective Breakability of Silica Nanocapsule

Given the lack of a selective response to GSH, a different synthesis scheme was attempted using TMOS instead of TEOS as organosilane precursor under the different BTSPD ratios summarized in Table 1 (vide supra). We hypothesized that introducing the shorter and less sterically hindered methyl group present in the TMOS would lead to more dense and stable structures. We followed two different approaches: (i) using higher amounts of precursors (i.e., using higher precursors to CytC ratios), to increase framework stability in the presence of DMEM and (ii) changing the BTSPD to TMOS ratio to tune the percentage of S—S bonds present in the silica framework, to achieve different release kinetics of the protein. TEM analysis confirmed the successful generation of smaller, denser, and more uniform nanocapsules with average diameters around 20 nm (see Figure 3a–c, Table 1, and Figure S2 DLS analyses), exhibiting less fragility and aggregation than their TEOS counterparts (Figure 2a–c). The three TM samples exhibited higher colloidal stability thanks to more negative ζ-potential values (increasing from 1-TM to 3-TM, Table 1). FT-IR spectra displayed in Figure 3d, revealed the same critical features for all the samples and the TE samples (vide supra), and TG analysis were identical for the three TM samples (Figure 3e). On the other hand, the encapsulation efficiency of CytC decreased, due to their smaller diameters and increased SiO_2 thickness, especially 1-TM and 2-TM samples (Figure TEM, Table 1).

In contrast to the TEOS samples, the TM samples maintained the sensitivity displayed by TEOS-based samples regarding breakability after exposure to the GSH concentration levels expected in the TME. Nevertheless, they exhibited a much higher resistance to DMEM culture medium, as can be seen by comparing the enlarged representations of the first 6 h of exposure (Figure S3). The results of Figure 3f show that by modifying the synthesis parameters the release sensitivity could be effectively tuned: thus, reducing the amount of disulfide bonds in the silica structure (i.e., moving from 1-TM to 2-TM) decreased somewhat the release rate in the presence of DMEM but the effect was minor. However, increasing the concentration of both precursors definitely improved the selectivity: while the total amount of protein released in the presence of GSH was similar for the three compositions tested, with the proportions used in 3-TM the unwanted release of CytC in the presence of DMEM was almost suppressed (Figure 3g).

TEM evaluation of the TM nanocapsules after exposure to GSH for 48 h confirmed their progressive degradation, the collapse and aggregation into an amorphous silica matrix (Figure 4a–c). Taking together, these results show how GSH has a strong degradation effect on the integrity of cleavable organosilica. This behavior is an important step toward the removal of nanoparticle fragments via two distinct pathways: renal clearance for fragments smaller than 6 nm, and hepatobiliary clearance for nanoparticles within the 6 to 50 nm range,[16] as summarized in Figure 4d. Overall, in terms of selective degradation the TMOS/BTSPD combination gives the best results, highlighting the feature of 3-TM to reach 48 h without significant release of Cyt C in the presence of cell culture medium. Furthermore, we investigated the response of this promising silica precursor's combination (3-TM) when exposed at different concentrations of GSH. Multiple and variable GSH levels are reported in the literature for both healthy and tumoral cell lines, respectively. The use of different analytical techniques also influences the final values detected, although HPLC and UPLC provide consensus of intracellular GSH concentrations between 5–10 mM in tumor cell lines.[4c,6a,17b,18a] Taking into account the average intracellular concentration found in different healthy cells types (0-2 mM)[18b–f] and the minimum threshold of tumoral cells, a CytC release kinetics at 48 h was evaluated both at GSH 1 mM and 5 mM (PBS 0.1 M pH = 7.4). Figure 3h reveals that at low concentrations of GSH as in healthy cells (2 mM or less)[18b–f] the conditions used to synthesize 3-TM were able to yield a material that was effective in preventing the release of the enclosed proteins over a 48 h period in the presence of 1 mM GSH or in DMEM. Furthermore, Figure 3i reveals that at the low concentrations of GSH (0-2 mM) representative of healthy cells,[18b–f] the release of proteins from the optimum 3-TM material was minimum (around 7%). We could therefore identify a strong GSH concentration dependence.

Finally, we investigated the stability of the systems developed by employing TMOS and BTSPD as breakable silica precur-

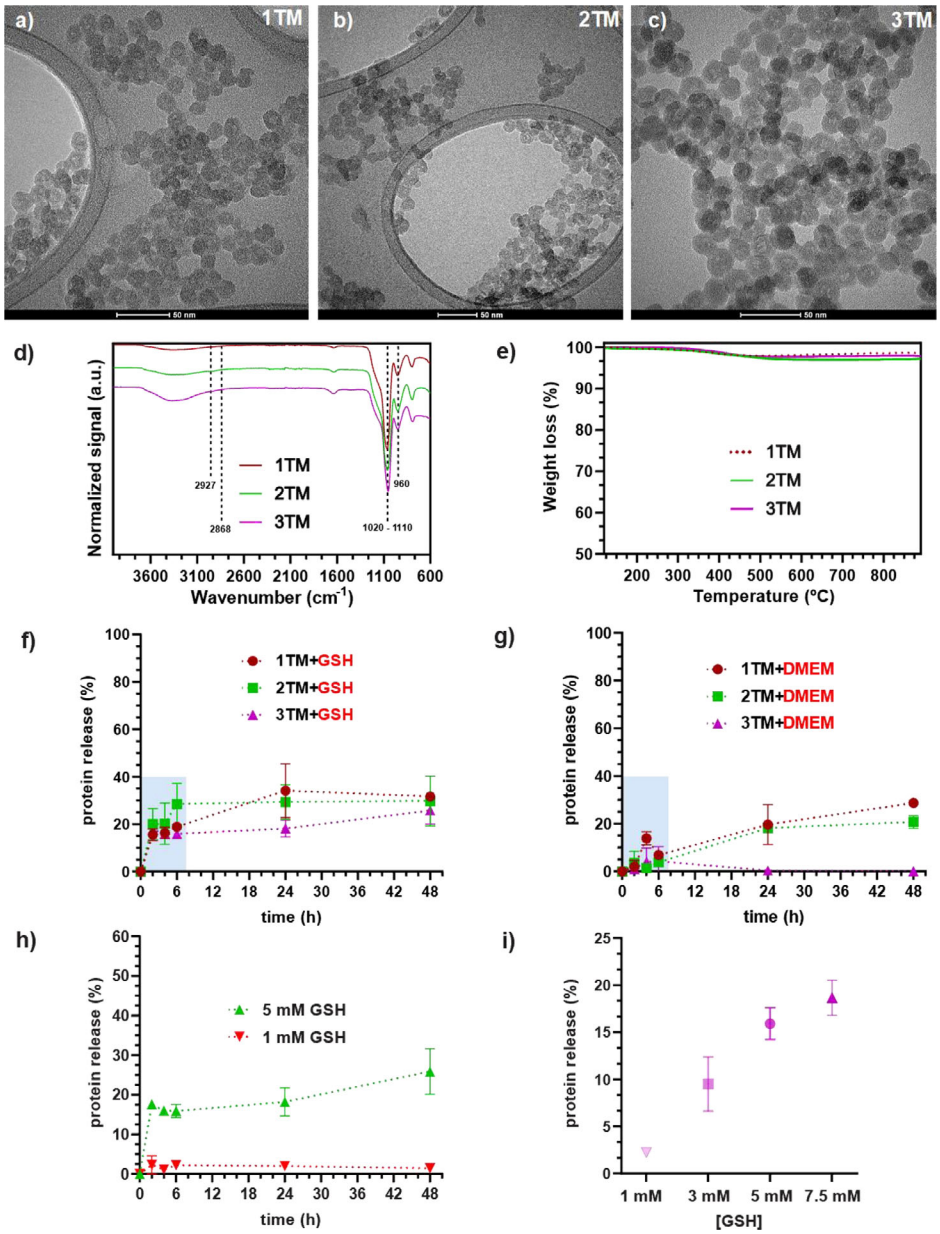

Figure 3. From (a–c) TEM of organosilica nanoparticles, images at 50 nm scale of syntheses using TMOS as silica precursor (1-TM, 2-TM, 3-TM, respectively) (d) FT-IR analysis of 1-TM, 2-TM, 3-TM. (e) Thermogravimetric analysis of organosilica NPs: syntheses using TMOS as precursor 1-TM (dot line), 2-TM (green line), and 3-TM (purple line). Release kinetics of CytC along 48 h: (f) 1-TM (brown line), 2-TM (green line), and 3-TM (purple line) in presence of GSH (5 mM in PBS 0.1 M pH = 7.4); (g) 1-TM (brown line), 2-TM (green line), and 3-TM (purple line) in presence of DMEM. (h) Release kinetics of 3-TM in presence of GSH 1 mM (red line) and 5 mM (green line) (in PBS 0.1 M pH = 7.4) along 48 h. (i) Percentage of protein released after 6 h under reducing conditions in presence of GSH 1 mM, 3 mM, 5 mM, 7.5 mM (in PBS 0.1 M pH = 7.4).

sors in water. TEM evaluation of the NPs after 1-month storage in water at 4 °C revealed no significant changes either in size or morphology (Figure S4). The stability of 3-TM, the most promising candidate, was also evaluated after storage in EtOH or acetonitrile (ACN) with no meaningful variations (see Figure S5).

3. Experimental Section

3.1. Materials

CytC from bovine heart, cyclohexane, *n*-hexanol, Triton 100X, TEOS (99%), TMOS (99%), glutathione reduced, sodium phosphate monobasic and dibasic, acetone, ethanol (EtOH) were purchased in Sigma–Aldrich–Merck. BTSPD (90%) was purchased in abcr. ACN (HPLC Quality) was purchased by WVR. Ultrapure water was prepared by Millipore IQ 7000 system. DMEM was purchased by ThermoFisher scientific, without phenol red and L-glutamine and containing sodium pyruvate and 4.5 g/L of Glucose.

3.2. Synthesis of Breakable Silica Nanoparticles

The initial protocol using TEOS as silica precursor, was adapted from a previous study.[10d] Typically, Triton X-100 (1.77 mL) and *n*-hexanol (1.8 mL) were dissolved in cyclohexane (7.5 mL). Separately, 600 µL of a solution of CytC (or water in case of empty nanocap-

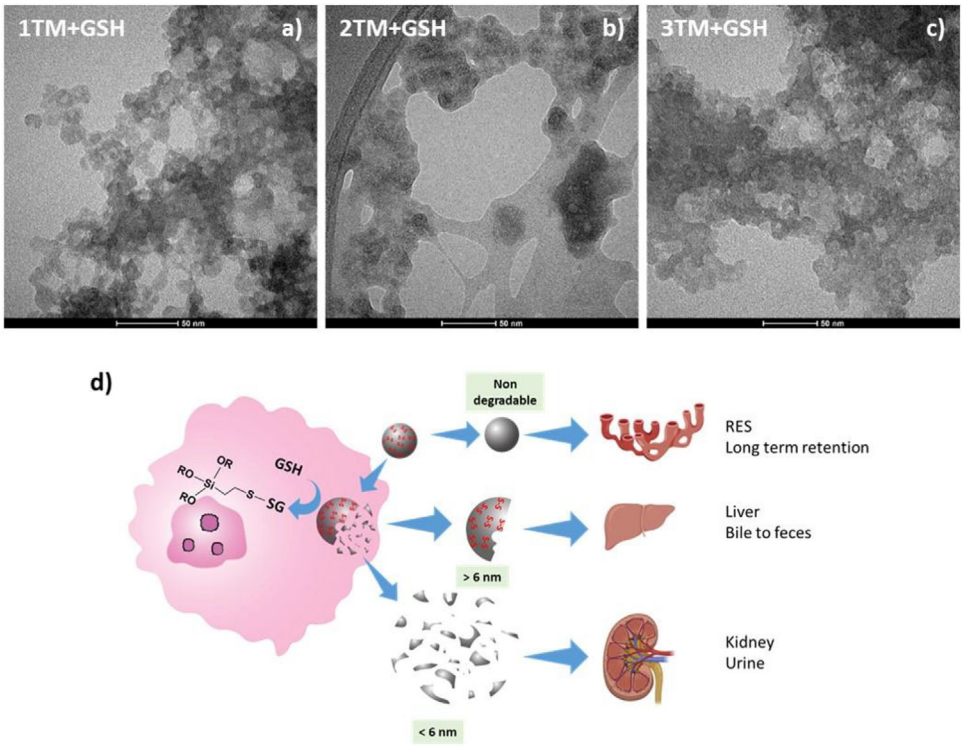

Figure 4. Evolution of TMOS derived nanocapsules after contact with GSH for 48 h: (a–c) TEM images of 1-TM, 2-TM, and 3-TM, respectively after 48 h; (d) Schematic display of expected clearance pathways of the capsules. Experimental conditions correspond to GSH 5 mM in PBS pH = 7.4 (0.1 M).

sules) (2.5 mg/mL) in water were mixed with 40 µL of TEOS and 60 µL of BTSPD. After briefly stirring up, this mixture was added to the organic solution. 50 µL of 30% aqueous ammonia solution was added and the water–oil emulsion was stirred overnight at room temperature at 350 rpm. A total of 20 mL of pure acetone was subsequently added in order to precipitate the NPs and the material was recovered by centrifugation, washing twice with ethanol and two times with ddH_2O. Final volume of resuspension were 2 mL of water. Further modification of the protocol in terms of silica precursor (TMOS) and amounts of reagents involved in the synthesis are summarized in Table 1 (vide supra). The synthesis of materials has been performed by the Platform of Production of Biomaterials and Nanoparticles of the NANBIOSIS ICTS, more specifically by the Nanoparticle Synthesis Unit (Unit 9) of the CIBER in BioEngineering, Biomaterials, and Nanomedicine (CIBER-BBN).

3.3. Characterization Techniques

SiO_2 nanocapsules were characterized after freeze-drying the samples. FT-IR analyses were performed using Bruker Vertex 70 equipment. TGA was carried out by using a protocol based on a gradient of 10 °C/min from 35 °C to 900 °C on a Mettler Toledo (TGA/SDTA851). Nanoparticles measured by FT-IR and TGA did not contain CytC to avoid signal interference in the silica framework due to the presence of the dye. Size and morphology were analyzed by performing TEM using a FEI TECNAI T20 microscope operated at 200 keV. Samples were prepared by drop casting aqueous suspensions of samples on holey carbon-Cu grids, 200 mesh, 50 microns. Size distribution was evaluated by measuring the diameters of nanoparticles on TEM images (n = 100) using Fiji ImageJ software and represented by frequency percentage distribution. ζ-potential evaluation was performed by a Z-Brookhaven 90 Plus in KCl 0.1 M solutions of the samples. DLS was performed on a Malvern Zetasizer by analyzing dispersions of NPs in water. Analyses were carried out with a laser angle of 173°, 3 runs, 15 repetitions for run, size distribution was analyzed by % in numbers.

3.4. Monitorization of CytC Release

In order to monitor the release of CytC from the nanocapsules, UV–vis analyses were carried out on a Jasco V670. The nanocapsules (0.5 mg/mL) were put in reaction with two different media: (i) GSH 5 mM to mimic concentration of reducing agent present in tumoral environment; (ii) DMEM to mimic the medium outside the cell membrane. To maintain neutral pH all over the experiment when using GSH, PBS 0.1 M at pH = 7.4 was used. The samples in reaction were kept at 37 °C in the dark. Absorbance readings were acquired at maximum absorbance peak at 410 nm using fixed wavelength method. Sample at 2, 4, 6, 24, and 48 h were centrifuged and measured the supernatant. In order to estimate the full release of CytC, 10 µL of NH_4OH were added to a solution of 0.5 mg/mL concentration of nanocapsules in order to reach strong basic pH conditions. Solution absorbance was then measured at 410 nm, and concentration calculated by Lambert–Beer law considering molar extinction coefficient ε_{410} = 106 000 M^{-1} cm^{-1}. To understand the influence of different GSH concentration and determine the threshold, GSH concentration levels at 1 mM, 3 mM, 5 mM, and 7.5 mM were used. To stabilize the pH value, PBS (0.1 M) at pH = 7.4 was employed.

3.5. Encapsulation and Loading Efficiency Calculations

In order to estimate the encapsulation efficiency and drug loading, 100% protein release was calculated as previously mentioned. Drug loading was estimated in terms of concentration (mg/mL) of protein

released from a solution of 0.5 mg/mL of nanocapsules in the presence of GSH 5 mM. Percentage w/w refers to total drug loading as follows:

$$\frac{\text{mgCytC}}{\text{mgNPs}} = \frac{\text{mg/mLCytCreleased}}{\text{0.5mg/mLNPs}}$$

$$\text{DrugLoading(\%)} = \frac{\text{mgCytC}}{\text{mgNPs}} \times 100$$

Encapsulation efficiency (EE) was defined as the amount of CytC encapsulated over the total CytC used for the synthesis (2.5 mg/mL in 0.6 mL). Considering average yield of synthesis as 15 mg/mL:

$$\text{encapsulatedCytC(mg)} = \frac{\text{mgCytC}}{\text{mgNPs}} \times \text{totalmgNPs}$$

$$\text{EE(\%)} = \frac{\text{encapsulatedCytC(mg)}}{\text{initialCytC}} \times 100$$

4. Conclusions

Replacing TEOS by TMOS as an alternative silica precursor in which the ethyl group is replaced by a methyl group as the ester derivative, allowed us to change the synthesis kinetics in the presence of BTSPD, leading to breakable SiO_2 nanocapsules with improved degradation characteristics. The encapsulation of CytC as a model therapeutic agent allowed us to monitor the kinetics of release and demonstrated a selective release only after exposure to threshold levels of GSH, typical of those found within the tumor environment. Interestingly, changing the proportion of S—S bonds precursor used in our synthesis did not induce large differences in terms of kinetic release or in the total amount of entrapped protein. The best results in terms of selective rupture were obtained with TMOS as silica precursor and with a BSTPD to TMOS molar ratio of 0.45.

Acknowledgments

The authors acknowledge financial support from the Spanish Ministry of Science, Innovation and Universities (FPI Ayuda PRE2022-104024 and Plan Nacional project CONCERT, PID2023-148732NB-I00). Luisa De Cola thanks the European Union´s Horizon 2020 research and innovation programme under grant agreement No 964386, project acronym "MimicKEY". The synthesis of materials has been performed by the Platform of Production of Biomaterials and Nanoparticles of the NANBIOSIS ICTS, more specifically by the Nanoparticle Synthesis Unit (Unit 9) of the CIBER in BioEngineering, Biomaterials & Nanomedicine (CIBER-BBN). The TEM studies were conducted at the Laboratorio de Microscopias Avanzadas, Instituto de Nanociencia y Materiales de Aragon, Universidad de Zaragoza, Spain. (SAI and ELECMI). Ayuda CEX2023-001286-S financiada por MICIU/AEI /10.13039/501100011033.

Conflict of Interests

The authors declare no conflict of interest.

Data Availability Statement

The data that support the findings of this study are available from the corresponding author upon reasonable request.

Keywords: Breakability · Glutathione · Proteins · Silica Capsules · Stimuli

[1] S. Charmsaz, D. M. Collins, A. S. Perry, M. Prencipe, *Cancers (Basel)* **2019**, *11*, 1125.
[2] a) M. F. Tang, L. Lei, S. R. Guo, W. L. Huang, *Chin. J. Cancer* **2010**, *29*, 775–780; b) G. Chen, I. Roy, C. Yang, P. N. Prasad, *Chem. Rev.* **2016**, *116*, 2826–2885.
[3] M. Huo, L. Wang, Y. Chen, J. Shi, *Nat. Commun.* **2017**, *8*, 357.
[4] a) J. I. Garcia-Peiro, J. Bonet-Aleta, M. L. Tamayo-Fraile, J. L. Hueso, J. Santamaria, *Nanoscale* **2023**, *15*, 14399–14408; b) M. C. Ortega-Liebana, J. Bonet-Aleta, J. L. Hueso, J. Santamaria, *Catalysts* **2020**, *10*, 333; c) J. Bonet-Aleta, M. Sancho-Albero, J. Calzada-Funes, S. Irusta, P. Martin-Duque, J. L. Hueso, J. Santamaria, *J. Colloid Interface Sci.* **2022**, *617*, 704–717.
[5] a) S. Gao, H. Lin, H. Zhang, H. Yao, Y. Chen, J. Shi, *Adv. Sci.* **2019**, *6*, 1801733; b) B. Yang, Y. Chen, J. Shi, *Chem. Rev.* **2019**, *119*, 4881–4985; c) B. Yang, Y. Chen, J. Shi, *Adv. Mater.* **2019**, *31*, 1901778.
[6] a) J. Bonet-Aleta, M. Encinas-Gimenez, E. Urriolabeitia, P. Martin-Duque, J. L. Hueso, J. Santamaria, *Chem. Sci.* **2022**, *13*, 8307–8320; b) B. Rubio-Ruiz, A. M. Perez-Lopez, L. Uson, M. C. Ortega-Liebana, T. Valero, M. Arruebo, J. L. Hueso, V. Sebastian, J. Santamaria, A. Unciti-Broceta, *Nano Lett.* **2023**, *23*, 804–811; c) M. Sancho-Albero, B. Rubio-Ruiz, A. M. Perez-Lopez, V. Sebastian, P. Martin-Duque, M. Arruebo, J. Santamaria, A. Unciti-Broceta, *Nat. Catal.* **2019**, *2*, 864–872.
[7] a) X. Liu, F. Wu, Y. Ji, L. Yin, *Bioconjugate Chem.* **2019**, *30*, 305–324; b) M. Zhu, X. Ding, R. Zhao, X. Liu, H. Shen, C. Cai, M. Ferrari, H. Y. Wang, R. F. Wang, *J. Controlled Release* **2018**, *272*, 72–82; c) B. G. Cha, J. H. Jeong, J. Kim, *ACS Cent. Sci.* **2018**, *4*, 484–492.
[8] T. Zhou, S. Yuan, P. Qian, Y. Wu, *Chem. Res. Chin. Univ.* **2023**, *39*, 72–82.
[9] a) W. Du, S. Du, X. Dong, H. Bai, J. Jiang, S. Hao, F. Yang, Q. Xiao, B. Zhang, J. Ge, L. Gao, L. Li, S. Q. Yao, W. Huang, *Biomaterials* **2023**, *294*, 122000; b) W. Fan, N. Lu, P. Huang, Y. Liu, Z. Yang, S. Wang, G. Yu, Y. Liu, J. Hu, Q. He, J. Qu, T. Wang, X. Chen, *Angew. Chem. Int. Ed. Engl.* **2017**, *56*, 1229–1233; c) D. Gößl, H. Singer, H.-Y. Chiu, A. Schmidt, M. Lichtnecker, H. Engelke, T. Bein, *New J. Chem.* **2019**, *43*, 1671–1680.
[10] a) J. G. Croissant, Y. Fatieiev, A. Almalik, N. M. Khashab, *Adv. Healthcare Mater.* **2018**, *7*, 1700831; b) Y. Zhang, B. Y. Hsu, C. Ren, X. Li, J. Wang, *Chem. Soc. Rev.* **2015**, *44*, 315–335; c) J. Zhu, Y. Niu, Y. Li, Y. Gong, H. Shi, Q. Huo, Y. Liu, Q. Xu, *J. Mater. Chem. B* **2017**, *5*, 1339–1352; d) E. A. Prasetyanto, A. Bertucci, D. Septiadi, R. Corradini, P. Castro-Hartmann, L. De Cola, *Angew. Chem., Int. Ed. Engl.* **2016**, *55*, 3323–3327; e) Y. Zhang, X. Lin, X. Chen, W. Fang, K. Yu, W. Gu, Y. Wei, H. Zheng, J. Piao, F. Li, *Int. J. Nanomed.* **2024**, *19*, 5859–5878.
[11] a) S. Murugadoss, D. Lison, L. Godderis, S. Van Den Brule, J. Mast, F. Brassinne, N. Sebaihi, P. H. Hoet, *Arch. Toxicol.* **2017**, *91*, 2967–3010; b) H. Mekaru, A. Yoshigoe, M. Nakamura, T. Doura, F. Tamanoi, *ACS Appl. Nano Mater.* **2018**, *2*, 479–488.
[12] a) D. Shao, F. Zhang, F. Chen, X. Zheng, H. Hu, C. Yang, Z. Tu, Z. Wang, Z. Chang, J. Lu, T. Li, Y. Zhang, L. Chen, K. W. Leong, W. F. Dong, *Adv. Mater.* **2020**, *32*, e2004385; b) Y. Yang, F. Chen, N. Xu, Q. Yao, R. Wang, X. Xie, F. Zhang, Y. He, D. Shao, W. F. Dong, J. Fan, W. Sun, X. Peng, *Biomaterials* **2022**, *281*, 121368; c) J. L. Vivero-Escoto, I. I. Slowing, C. W. Wu, V. S. Lin, *J. Am. Chem. Soc.* **2009**, *131*, 3462–3463.
[13] a) S. Wilhelm, A. J. Tavares, Q. Dai, S. Ohta, J. Audet, H. F. Dvorak, W. C. W. Chan, *Nat. Rev. Mater.* **2016**, *1*, 16014; b) J. Florek, R. Caillard, F. Kleitz, *Nanoscale* **2017**, *9*, 15252–15277; c) M. Vallet-Regi, M. Colilla, I. Izquierdo-Barba, M. Manzano, *Molecules* **2017**, *23*, 47.

[14] a) X. Tang, Z. Wang, Y. Xie, Y. Liu, K. Yang, T. Li, H. Shen, M. Zhao, J. Jin, H. Xiao, H. Liu, N. Gu, *ACS Nano* **2023**, *17*, 4062–4076; b) Y. Wang, Y. Xie, K. V. Kilchrist, J. Li, C. L. Duvall, D. Oupicky, *ACS Appl. Mater. Interfaces* **2020**, *12*, 4308–4322; c) S. Wang, X. Liu, S. Chen, Z. Liu, X. Zhang, X. J. Liang, L. Li, *ACS Nano* **2019**, *13*, 274–283.

[15] a) H. Yamauchi, T. Ishikawa, S. Kondo, *Colloids Surf.* **1989**, *37*, 71–80; b) R. Lindberg, J. Sjöblom, G. Sundholm, *Colloids Surf. A:Physicochem. Eng. Asp.* **1995**, *99*, 79–88; c) K. Osseo-Asare, F. J. Arriagada, *Colloids Surf.* **1990**, *50*, 321–339.

[16] a) L. Wang, W. Tan, *Nano Lett.* **2006**, *6*, 84–88; b) M. Qhobosheane, S. Santra, P. Zhang, W. Tan, *Analyst* **2001**, *126*, 1274–1278; c) S. Santra, R. Tapec, N. Theodoropoulou, J. Dobson, A. Hebard, W. Tan, *Langmuir* **2001**, *17*, 2900–2906; d) S. Santra, P. Zhang, K. Wang, R. Tapec, W. Tan, *Anal. Chem.* **2001**, *73*, 4988–4993; e) S. Santra, K. Wang, R. Tapec, W. Tan, *J. Biomed. Opt.* **2001**, *6*, 160–166.

[17] a) J. Bonet-Aleta, J. L. Hueso, L. Sanchez-Uriel, M. Encinas-Gimenez, S. Irusta, P. Martin-Duque, G. Martinez, J. Santamaria, *Mater. Today Chem.* **2023**, *29*, 101404; b) J. Bonet-Aleta, J. V. Alegre-Requena, J. Martin-Martin, M. Encinas-Gimenez, A. Martin-Pardillos, P. Martin-Duque, J. L. Hueso, J. Santamaria, *Nano Lett.* **2024**, *24*, 4091–4100; c) L. Sanchez-Uriel, J. Bonet-Aleta, A. Ibarra, J. L. Hueso, *J. Phys. Chem. C:Nanomater. Interfaces* **2023**, *127*, 14146–14154.

[18] a) C.-Y. Cui, B. Li, X.-C. Su, *ACS Cent. Sci.* **2023**, *9*, 1623–1632; b) H. Vázquez-Meza, M. M. Vilchis-Landeros, M. Vázquez-Carrada, D. Uribe-Ramírez, D. Matuz-Mares, *Antioxidants* **2023**, *12*, 834; c) J. C. Jean, Y. Liu, L. A. Brown, R. E. Marc, E. Klings, M. Joyce-Brady, *Am. J. Physiol. Lung Cell Mol. Physiol.* **2002**, *283*, L766-L776; d) A. M. Cantin, S. L. North, R. C. Hubbard, R. G. Crystal, *J. Appl. Physiol.* **1987**, *63*, 152–157; e) D. Giustarini, A. Milzani, I. Dalle-Donne, R. Rossi, *Blood Cells, Mol., Dis.* **2008**, *40*, 174–179; f) S. Li, X. Li, G. J. Rozanski, *J. Mol. Cell. Cardiol.* **2003**, *35*, 1145–1152.

[19] a) Q. Wei, Y. Chen, X. Ma, J. Ji, Y. Qiao, B. Zhou, F. Ma, D. Ling, H. Zhang, M. Tian, J. Tian, M. Zhou, *Adv. Funct. Mater.* **2018**, *28*, 1704634; b) H. P. Rim, K. H. Min, H. J. Lee, S. Y. Jeong, S. C. Lee, *Angew. Chem., Int. Ed. Engl.* **2011**, *50*, 8853–8857; c) Z. Teng, W. Li, Y. Tang, A. Elzatahry, G. Lu, D. Zhao, *Adv. Mater.* **2019**, *31*, e1707612; d) X. Du, F. Kleitz, X. Y. Li, H. W. Huang, X. J. Zhang, S. Z. Qiao, *Adv. Funct. Mater.* **2018**, *28*, 1707325.

[20] a) J. Croissant, X. Cattoen, M. W. Man, A. Gallud, L. Raehm, P. Trens, M. Maynadier, J. O. Durand, *Adv. Mater.* **2014**, *26*, 6174–6180; b) D. Wang, Z. Xu, Z. Chen, X. Liu, C. Hou, X. Zhang, H. Zhang, *ACS Appl. Mater. Interfaces* **2014**, *6*, 12600–12608.

[21] P. Picchetti, G. Moreno-Alcantar, L. Talamini, A. Mourgout, A. Aliprandi, L. De Cola, *J. Am. Chem. Soc.* **2021**, *143*, 7681–7687.

[22] a) Y. Yang, J. Wan, Y. Niu, Z. Gu, J. Zhang, M. Yu, C. Yu, *Chem. Mater.* **2016**, *28*, 9008–9016; b) K. Wang, X. Li, H. Wang, H. Lu, D. Di, Q. Zhao, S. Wang, *Colloids Surf. A:Physicochem. Eng. Asp.* **2021**, *608*, 125566; c) P. Huang, X. Qian, Y. Chen, L. Yu, H. Lin, L. Wang, Y. Zhu, J. Shi, *J. Am. Chem. Soc.* **2017**, *139*, 1275–1284; d) P. Huang, Y. Chen, H. Lin, L. Yu, L. Zhang, L. Wang, Y. Zhu, J. Shi, *Biomaterials* **2017**, *125*, 23–37.

[23] A. Lerida-Viso, A. Estepa-Fernandez, A. Garcia-Fernandez, V. Marti-Centelles, R. Martinez-Manez, *Adv. Drug Delivery Rev.* **2023**, *201*, 115049.

Manuscript received: November 22, 2024
Revised manuscript received: May 30, 2025
Accepted manuscript online: June 11, 2025
Version of record online: ■■, ■■